J Electr Eng Technol.2017; 12(5): 1842-1850
http://doi.org/10.5370/JEET.2017.12.5.1842

ISSN(Print) 1975-0102
ISSN(Online) 2093-7423

Structural Design for Vibration Reduction in Brushless DC Stator

Mehrdad Jafarboland† and Hossein Bagherian Farahabadi*

Abstract – Reducing the noise and vibration of the BLDC motors is very essential for some special applications. In this paper, a new structural design is introduced to increase the natural frequencies of the stator in BLDC motors as increasing the natural frequencies can reduce the severe effects of the structural resonances, including high levels of noise and vibration. The design is based on placing a single hole on definite regions at the stator cross sectional area (each region contains one tooth and its upper parts in the stator yoke) in an optimum way by which the natural frequencies at different modes are shifted to the higher values. The optimum diameter and locations for the holes are extracted by the Response Surface Methodology (RSM) and the modal analyses in the iterative process are done by Finite Element Method (FEM). Moreover, the motor performance by the optimum stator structure is analyzed by FEM and compared with the prototype motor. Preventing the stator magnetic saturation and the motor cogging torque enhancement are the two constraints of the optimization problem. The optimal structural design method is applied experimentally and the validity of the design method is confirmed by the simulated and experimental results.

Keywords: BLDC stator, Hole placement, Modal analysis, Natural frequencies, Structural design

1. Introduction

Brushless DC (BLDC) motors are among the most applicable motors in various industries. They are used in many applications nowadays. Calm and quiet operation of the BLDC motors is generally needed in various applications, but in some especial cases, it is essential. Therefore, various studies have been done in this field and different ways of reducing the noise and vibration have been introduced. Nevertheless, applying different ways of reducing the noise and vibration in the motor design and construction process without paying attention to reducing or eliminating the effects of structural resonances is not reasonable. This is due to the severe effects of the resonance occurrence. Structural resonance causes high levels of noise and vibration that overcomes the reductions achieved by applying different methods of reducing the noise and vibration.

Some researchers have worked on the mentioned issue and their works have been done for different kinds of motors such as permanent magnet (PM) ones.

A method to decrease the magnetically induced vibrations of a PM motor is introduced in [1] which is developed by performing magnetic and structural finite element (FE) analyses and optimization. The motor vibrations caused by the magnetic forces were extracted by the mode superposition method. The results were experimentally validated.

The stator natural frequencies were compared with the radial forces acting on the stator in [2]. An experimental investigation about the effects of the structural dynamic characteristics, like the mode shapes and natural frequencies and the electromagnetic excitation forces, on a PM motor vibrations and noise is reported in the study. In [3] a new design (including electromagnetics and structural parts) is developed in order to decrease the noise in a prototype PM motor. In the electromagnetic design part, the harmonic amplitude of magnetic forces influences the teeth and the torque ripple are decreased by an optimal method. In the structural part of the design, the natural frequencies were shifted to higher values to increase the stiffness of the stator structure.

Some of the natural frequencies of a prototype stator structure are derived by simulation and experimental test in [4]. The characteristics of the tangential and radial magnetic forces applied on the stator teeth in a PM motor and the magnetically induced vibrations are investigated in the study under flux weakening control.

The stator vibration caused by the radial forces is studied in [5] and an improved stator model is introduced. The vibration of the prototype and improved models were evaluated by both FEM and experimental tests. In [6] a structural FE model of a PM motor is introduced which includes stiffness of ball bearings and verified by comparing the natural frequencies derived by simulations and experimental tests. The magnetic forces are extracted and then transformed into the nodal forces and the vibrations of the prototype interior PM motor are investigated.

The natural frequencies of the systems can be modified by changing some objects that have definite effects on the size, inertia or forces of the systems. The circumferential

† Corresponding Author: Malek-Ashtar University of Technology, Iran. (j_mehrdad405@hotmail.com)
* Malek-Ashtar University of Technology, Iran. (hbaqerian@gmail.com)
Received: November 15, 2016; Accepted: May 16, 2017

vibration modes can have different values form 0 to ∞. The lower mode numbers are more important than the higher ones as the natural frequencies at higher mode numbers might be out of the concerned range [7].

In this paper, a new structural design is presented in order to shift the natural frequencies of a prototype stator of a BLDC motor to higher values and increase the stator's stiffness. When one of the frequency components of an excitation force coincides with one of the natural frequencies of the BLDC motor with modified stator structure and the structural resonance occurs, the produced noise and vibration have lower intensities as the force component magnitude has lower value at higher frequencies. The stator structure modification can also omit the resonance occurrence in some cases.

The modal analysis in this study is done by the Solidworks software which is based on the Finite Element Analysis (FEA). In this software, an Eigen value approach is used to determine the natural vibration modes for different geometries. The proposed structural design can be applied in the design stage of the stator for all types of electric motors such as BLDC ones.

The new structural design is based on placing a single hole, with definite diameter and location, on definite regions at the stator cross sectional area. Each region contains a tooth and its upper part at the stator yoke. The diameter and locations of the holes are calculated by RSM in a cylindrical coordinates and the modal analyses in the iterative process are done by FEM. Preventing the stator structure magnetic saturation and the motor cogging torque enhancement are the optimization problem constraints which are evaluated by the motor performance derived by FEM. The design method validity is tested and confirmed experimentally.

2. Theory

2.1 Excitation forces

The noise and vibration produced during the motor operation is caused by the excitation forces [8] and these forces have different origins. The frequency components of electromagnetic excitation forces in the BLDC motors are given here. The Frequencies of the radial magnetic force components can be calculated by:

$$f_r = n \times P \times X \tag{1}$$

Where n is an integer (representing the harmonic number), P and X are the motor pole numbers and its rotating frequency, respectively. The frequencies of the tangential magnetic force components are:

$$f_t = n \times G \times X \tag{2}$$

where G is the least common multiplier of the motor's poles and slots numbers.

The frequencies of the excitation force components generated by the switching process are:

$$f_s = n \times 3P \times X \tag{3}$$

The leading harmonic order of the vibration obtained by the superimposition of each excitation harmonic order can be expressed as:

$$f_{exc} = n \times LCM(f_r, f_t, f_s) \tag{4}$$

In Eq. (4), LCM stands for least common multiplier. Eq. (4) expresses an essential harmonic component of the vibration generation as shown in the next Eq. (9).

$$G^{th} = LCM(f_r, f_t, f_s) / P \tag{5}$$

2.2 Natural frequencies of the stator core

In this section, the modal vibration behavior of the stator structure is discussed analytically. An analytical approach for calculating the stator core's natural frequencies are investigated and its accuracy is discussed. The natural frequency of the mth circumferential vibrational mode of the stator structure can be calculated by [8]:

$$f_m = \frac{1}{2\pi}\sqrt{\frac{K_m^{(c)}}{M_c}} \tag{6}$$

$K_m^{(c)}$ (N/m) and (kg) in Eq. (6) are the lumped stiffness and the lumped mass of the stator structure respectively. If the stator structure is considered as a cylindrical shell with infinite length, the natural frequency of the system for the mth circumferential mode can be calculated by [10]:

$$f_m = \frac{\Omega_m}{\pi D_c}\sqrt{\frac{E_c}{\rho_c(1-\nu_c^2)}} \tag{7}$$

Where E_c is the elasticity modulus, ρ_c is the mass density, D_c is the stator mean diameter, ν_c is the Poisson ratio for the stator core and Ω_m is the roots of the characteristic equation of motion. According to the Donnel-Mushtari theory [8], Ω_m is 1 for the circumferential mode m=0 ($\Omega_m = 0$) and for the circumferential modes $m \geq 1$ is:

$$\Omega_m = \sqrt{\frac{1}{2}((1+m^2+\kappa^2 m^4) \pm \sqrt{(1+m^2+\kappa^2 m^4)^2 - 4\kappa^2 m^4})} \tag{8}$$

Where the parameter κ^2 is $\frac{h_c^2}{3D_c^2}$ in which h_c is the

stator yoke thickness.

The lumped stiffness and mass can be expressed in the forms of the Eqs. (9) and (10) if we want to show Eq. (7) in the form of Eq. (6):

$$K_m^{(c)} = \frac{4\Omega_m{}^2}{D_c}\frac{\pi L_i h_c E_c}{1-\nu_c{}^2} \quad (9)$$

$$M_c = \pi \rho_c D_c L_i h_c \quad (10)$$

L_i in the Eqs. (9) and (10) is the effective length of the stator core [8].

In the stator core, the windings are located in slots which are separated by the steel teeth. The tooth-slot zone with the windings can be considered as an additional ring internal to the stator core (yoke). The natural frequency of the stator system with the windings can be calculated by:

$$f_m = \frac{1}{2\pi}\sqrt{\frac{K_m^{(c)} + K_m^{(w)}}{M_c + M_w}} \quad (11)$$

Where $K_m^{(c)}$ (N/m) and (kg) are defined like Eq. (6), $K_m^{(w)}$ is the lumped stiffness of tooth-slot zone including the windings and M_w is the mass of the teeth, windings, and insulation.

In order to extract the equations for the natural frequencies of stator structure, the analytical equations should be written for a cylindrical shell, but because of the shell's curvature, a coupling exists among the vibrations in the radial, axial and tangential directions. Therefore, the excitations in one direction cause vibrations in the three mentioned directions and this is more dominant at lower frequencies. Thus, many simplifications and approximations are needed in the analytical solution process and solving the vibration equations directly is so hard [11] and hence the accuracy of the analytical solution is low. Consequently, in this study, to consider the effects of the structural modifications in the stator, the low accuracy of the analytical solutions makes them insufficient to be used and the numerical approaches should be applied. Therefore, the finite element method is used for the analyses of this study.

The rotor natural frequencies can also be derived independently. The natural frequencies of a system can be calculated by the mode superposition method [8].

2.3 Amplitude of vibration displacements

The amplitude of vibration displacements of the mth vibrational mode can be calculated by:

$$A_m = \frac{F_m / M}{\sqrt{(\omega_m{}^2 - \omega_r{}^2)^2 + 4\zeta_m{}^2 \omega_r{}^2 \omega_m{}^2}} \quad (12)$$

In Eq. (12), M is the mass (kg) of the shell with cylindrical shape (by which the stator is modeled), ω_m and ω_r are the angular natural frequency of the mth mode and the angular frequency of the force component with order r respectively, and ζ_m is the modal damping ratio. F_m is the amplitude of force which can be calculated by:

$$F_m = \pi D_{1in} L_i P_{mr} \quad (13)$$

Where D_{1in} and L_i are the stator core's inner diameter and its effective length, respectively, and P_{mr} is the magnetic pressure magnitude with order r [8]. Determining the modal damping ratio ζ_m by analytical methods is not straightforward and generally its determination is done by the experimental methods [8]. An equation derived from the experimental methods, which is for electric machines with small and medium sizes, is expressed as [12]:

$$\zeta_m = \frac{1}{2\pi}(2.76\times10^{-5} f_m + 0.062) \quad (14)$$

Where f_m (Hz) is natural frequency of mode m. Considering Eq. (12), it can be claimed that when the frequency of the excitation force component is close to one of the natural frequencies of the stator structure, maximum vibration and noise can be produced. Therefore, in the stator vibration analysis, considering the electromagnetic force components which their frequencies are close to the natural frequencies of the stator structure may be enough [8].

3. Structural Design

In this section, an optimized structural design approach is introduced to move the structural resonances of the stator structure to higher frequencies in order to enhance the stiffness. As mentioned before, the approach contains holes placement on definite regions of the stator cross sectional area in an optimum way by using response surface methodology (RSM) and checking the performances of the prototype and optimal motors by FEM.

3.1 Modeling of the stator

The prototype motor which is modeled for this study is a 4000 rpm BLDC motor with 10 poles and 12 slots. The specifications of the modeled stator are shown in Table 1. The steel type is ASTM-A677 which is the product of the

Table 1. The modeled stator specifications

Outer Diameter	52.4 mm
Inner Diameter	25.7 mm
Length	24.5 mm
Number of Slots	12
Steel Type	ASTM-A677-64F200 Product of Cogent Co.

Table 2. The properties of the stator material

Property (unit)	Value	
Young modulus (psi)	Rolling direction	2.68e10
	Transverse direction	2.97e10
Poisson's ratio	0.29	
Shear modulus (psi)	11501492.6	
Mass density (Kg/ m^3)	7600	
Tensile strength (psi)	71000	
Yield strength (psi)	54300	

Table 3. The natural frequencies of the prototype stator

Mode number	Natural frequency (Hz)	Mode number	Natural frequency (Hz)
1	1368.6	6	6010.8
2	2113.5	7	8206.9
3	4598.2	8	8570.7
4	5258.8	9	10409
5	5259.2	10	10411

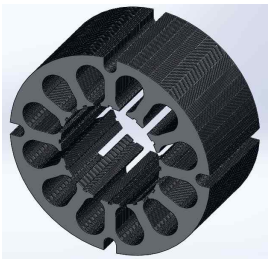

Fig. 1. The prototype stator structure

Cogent Company (64F200). The steel thickness is 0.0250 inch. The material properties of the steel are presented in Table 2 (extracted from the product's brochure).

The stator structure with its mentioned detailed specifications and material properties has been modeled in the Solidworks software environment.

One of the unique features of this study is the accurate modeling of the laminated stator structure in the software. In [6] the laminated structure of the motor is modeled by using an orthotropic material, but in this study the laminations are directly applied in the modal analysis. The modeled structure is shown in Fig. 1. Note that the laminations in the model are bonded to each other.

Considering the poles and slots numbers and the rated speed, the upper bound frequency in the modal analysis is selected near 10 KHz because the frequency components of the excitation forces in the motor do not have considerable values in the ranges above 10 KHz. The upper bound frequency for the study is obtained according to the results presented in [13].

The natural frequencies of the prototype stator structure are presented in Table 3 (only the elastic modes are presented).

Considering Eqs. (1) to (3), we have P=10, S=12 and X=66.67 Hz. The frequency components of the different types of forces produced in the prototype BLDC motor

Table 4. The frequency values for the components of the electromagnetic forces in the BLDC motor.

No.	Frequency (Hz)	Type	No.	Frequency (Hz)	Type
1	667	r*,t**,s***	9	6000	r, s
2	1333	r	10	6667	r
3	2000	r, s	11	7334	r
4	2667	r	12	8000	r, t, s
5	3333	r	13	8667	r
6	4000	r, t, s	14	9334	r
7	4667	r	15	10001	r, s
8	5334	r	*radial, **tangential, ***switching		

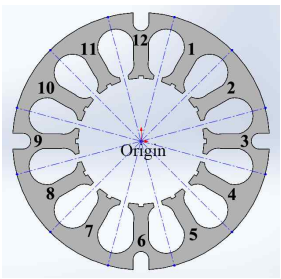

Fig. 2. The stator cross sectional area regions in the structural design

have overlaps at some frequencies. The frequencies of the different force components up to 10 KHz (the selected upper bound frequency) are presented in Table 4. The excitation force types (radial, tangential and switching) are defined for each frequency component.

As mentioned before, considering the electromagnetic force components which their frequencies are close to the natural frequencies of the stator structure may be enough in the stator vibration analysis.

3.2 Structural design approach

In this part, for the stator which is modeled in the software, the new structural design has been applied by which the natural frequencies at different mode shapes are shifted to higher values, and the stator stiffness is increased. As mentioned before, the design is based on placing a hole with definite diameter and location on specific regions at the stator cross sectional area. Each region contains one stator tooth with its upper parts in the stator yoke. The regions for the prototype stator are shown in Fig. 2.

Preventing the stator structure with holes from magnetic saturation is considered as a constraint for the problem. The other constraint is preventing the motor cogging torque increment as placing the holes causes some changes in the reluctance of the passes which the magnetic flux follows. The mentioned constraints have been applied by checking the motor performance by FEM.

The locations and diameters of the holes are defined by the RSM, and the modal analyses in the iterative process of the optimization algorithm are done by FEM. In RSM, the

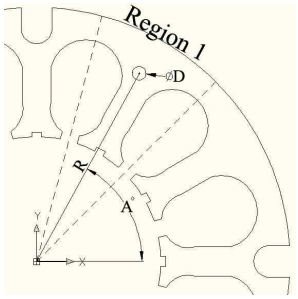

Fig. 3. The optimization parameters used for RSM

hole's optimum location is extracted by defining different locations of the hole in a cylindrical coordinate system with the stator center as the origin. The parameters which are used for RSM are shown in Fig. 3.

In Fig. 3, "D" is the diameter of the hole, "R" is the distance between the center of the hole and the coordinate system origin and "A" is the angle which is defined in the cylindrical coordinate system.

The minimum and maximum diameters of the holes are set at 0.5 mm and 1.5 mm for the algorithm, respectively. For the prototype stator structure, placing holes with diameters smaller than 0.5 mm does not have any considerable effects on the natural frequencies. Also, placing holes with diameters larger than 1.5 mm might cause magnetic saturation of the stator. The diameters of the holes are modified by 0.1 mm steps during the iterative process in the optimization algorithm. The modification steps for the parameters "R" and "A" are 0.2 mm and 1 degree, respectively.

The constraints for parameters "D", "R" and "A" are given in Eqs. (15) to (17). Note that the optimum values which are derived for the parameters in region 1 (considering Figs. 2 and 3) are used to derive the hole diameter and location at the other regions ("D" and "R" are the same at different regions and "A" is subtracted by 30 degrees for region 2; added by 30 degrees for region 12, 60 degrees for region 11, etc.).

$$0.5mm \le D \le 1.5mm \quad (15)$$

$$13mm \le R \le 26mm \quad (16)$$

$$45° \le A \le 75° \quad (17)$$

It should be noted that in the response surface design process for the prototype stator, the minimum and maximum values for "A" depend on the value of "R". For example, when "R" is lower than 24 mm, the permitted range for the changes of "A" decreases in comparison with Eq. (17).

For region 1 the optimum values of the parameters are presented in Table 5 and for the other regions, the parameters can be derived using the values in this table. The results show that the optimum hole locations are where the holes' centers are located on the stator's radii going through the stator teeth tip centers (for all of the regions).

Table 5. The optimum values of the parameters.

Parameter	Value
D	1 mm
R	23.6 mm
A	60°

Table 6. The natural frequencies of the optimum stator

Mode number	Natural frequency (Hz)	Mode number	Natural frequency (Hz)
1	1559.4	6	6236.3
2	2314.1	7	8449.5
3	4801	8	8814.9
4	5478	9	10660.1
5	5478.9	10	10663.4

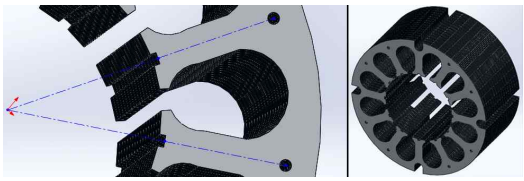

Fig. 4. The optimum stator model with holes

The optimum model in the software environment is shown in Fig. 4.

The natural frequencies of the optimum stator structure are presented in Table 6 (only the elastic modes are presented). As mentioned before, the upper bound frequency is near 10 KHz.

The natural frequencies of the prototype and the optimum stator structures can be calculated theoretically by Eqs. (6) to (10). Considering the parameters in the equations, it can be seen that the calculated natural frequencies will be the same for the both stators despite their structural differences caused by placing the holes. This shows the insufficient accuracy of the theoretical equations for this study and therefore only the numerical methods like FEM can be used for the case.

The results in Tables 3 and 6 show that the natural frequencies at all mode shapes increase by placing the holes with optimum diameter and locations.

Considering Tables 3 and 6, the frequency components which are close to the natural frequencies of the prototype and optimum stator structures are extracted from Table 4. Then by using Eqs. (12) to (14), the amount of vibration displacements amplitude reduction achieved by placing the holes with the optimum diameters and locations on the stator regions is calculated. Considering the reduction at different mode shapes, the amplitude of the vibration displacements decreases about the total average of 56% in the optimum stator structure compared to the prototype one.

In order to progress the problem constraints, the motor with the optimum stator structure derived by RSM and the modal analysis is analyzed by FEM to evaluate its performance in comparison with the prototype motor. The results show that placing the holes does not cause the stator

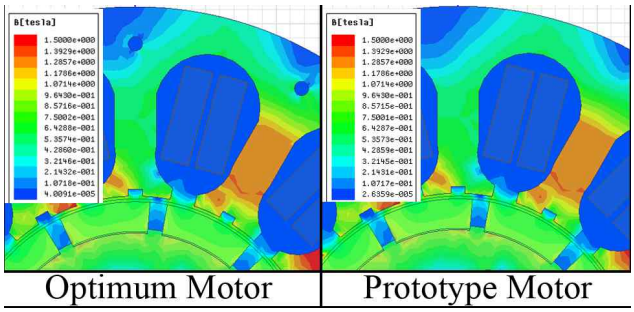

Fig. 5. The magnetic flux densities in the motors

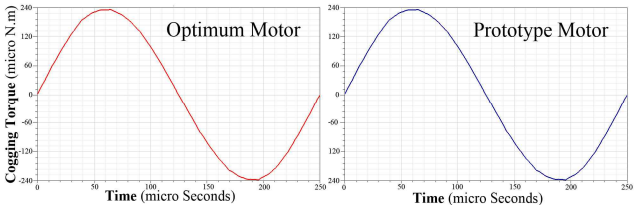

Fig. 6. The cogging torque profile versus time in the motors with the prototype and optimum stators

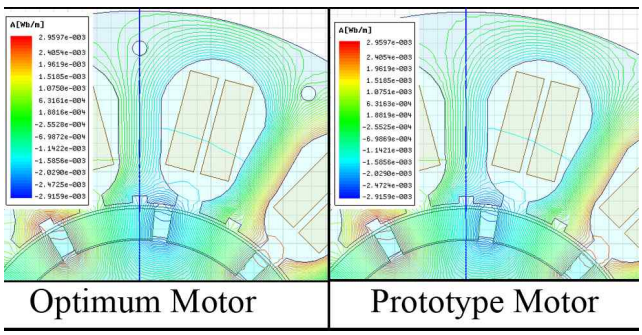

Fig. 7. The magnetic flux lines in the motors

magnetic saturation (the stator maximum magnetic flux density is about 1.5 Tesla). The magnetic flux densities on the two motor' cross sectional areas are shown in Fig. 5.

Considering Fig. 5, it can be seen that the expected partial magnetic saturation around the hole is negligible.

The results of the analysis also show that placing the holes with optimum diameters and locations does not increase the motor cogging torque. The cogging torque profiles and their peak to peak values (about 0.48 mN.m) are the same for the two motors according to the FEM results. The cogging torque profile versus time in the motors with the prototype and optimum stators are shown in Fig. 6.

Comparing the performances of the prototype and the optimum motors also shows that placing the optimal holes does not cause any important changes in the motor performance and no penalties exist for the proposed structural design.

The magnetic flux lines on the two motors' cross sectional area are shown in Fig. 7.

The flux lines characteristics in Fig. 7 shows that placing

Table 7. FEA results for the prototype and optimum motors

Parameter	Prototype Motor	Optimum Motor
Output speed (rpm)	3998	4007
Output torque (N.m)	0.401	0.4
Torque ripple (%)	6	6.1
Efficiency (percent)	86.9	86.9

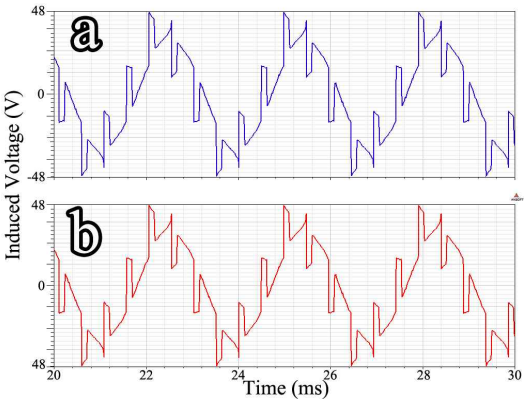

Fig. 8. Back EMF waveforms for one phase: (a) prototype motor, (b) optimum motor

the optimum holes does not cause important disturbances in the flux continuity. The back EMF waveforms of the two motors, for one phase, are shown in Fig. 8. As can be seen in Fig. 8, the back EMF waveforms for the two motors in the same phase are exactly similar.

The efficiency, output torque, speed and other characteristics of the prototype and optimum motors are the same according to the FEA results. Some of the analysis results are presented in Table 7.

Comparing the results in Table 7 shows that the optimization process does not have any negative influences on the motor performance.

4. Experimental Verifications

In order to validate the proposed structural design experimentally, two BLDC motors were designed and constructed. The components and structures of the two motors were the same except for the stator structures. The studied prototype stator structure and the optimum stator structure with holes were used in the two motors.

The motors with their stator structures are shown in Fig. 9. Some of the holes on the optimal motor's stator are shown in Fig. 9(b). The other holes on the optimum stator cross sectional area have been covered during the motor winding process. One of the core laminates of the two stators are shown in Fig. 9(c).

The vibration spectrum of the two constructed motors have been measured and recorded in the frequency range 0-16 KHz. The upper bound frequency in the measurement has been selected more than the maximum interested

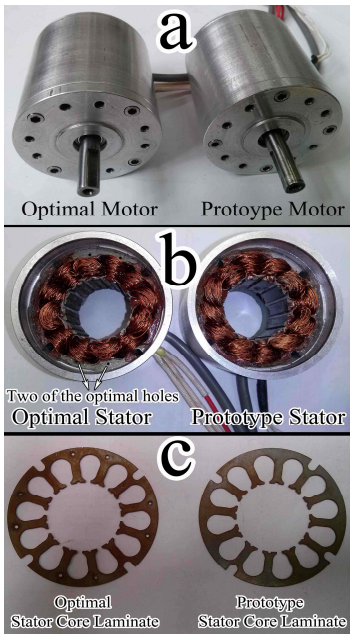

Fig. 9. (a) The prototype and optimum constructed motors; (b) The prototype and optimum stator structures used in the motors; (c) One of the core laminates of the two stators.

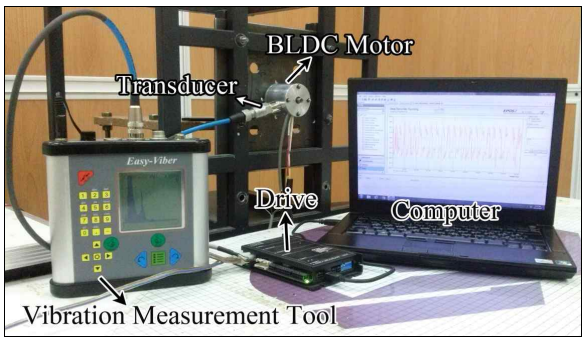

Fig. 10. The motors vibration spectrum measurement setup

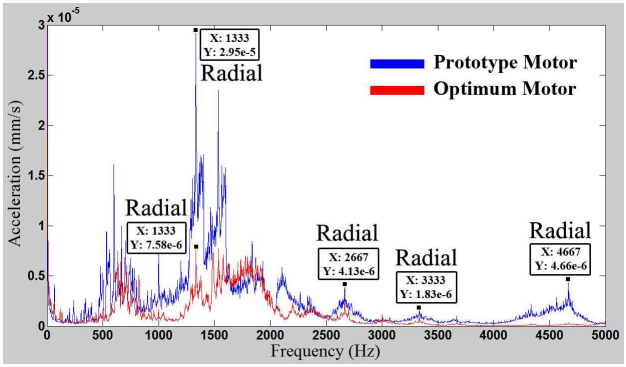

Fig. 11. The vibration spectrum of the prototype and the optimum motors at 4000 rpm

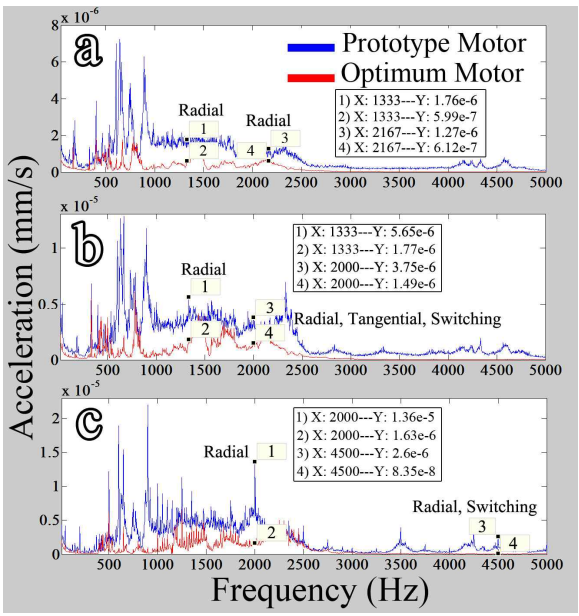

Fig. 12. The vibration spectrum of the prototype and the optimum motors at different speeds, a)1000 rpm, b) 2000 rpm, c)3000 rpm

frequency to confirm that no important component remains in the frequencies greater than 10 KHz. The two motors' vibration spectrum has been measured at the motor rated speed 4000 rpm and their vibration spectrum measurement setup is shown in Fig. 10.

The vibration spectrum of the prototype and the optimal motor at the rated speed are shown in Fig. 11. The vibration spectrum over the 5000 Hz had negligible amplitude and has not been shown in the figure.

As can be seen in Fig. 11, the vibration components' amplitude in the optimal motor has decreased at most of the frequencies. Also, it can be seen that a resonance occurs at 1333 Hz in the prototype motor which is due the interference between the radial magnetic force component and the natural frequency of the motor. Considering the figure, it can be seen that as the natural frequency at the first elastic mode has been shifted to an upper value at the optimum motor, the resonance occurrence has been disappeared in this motor (the motor accelerations is about 4 times smaller for the optimum motor). Similar conditions exist at the frequency 4667 Hz in the prototype motor and a resonance with lower severity occurs (as the excitation force components have lower magnitudes at higher frequencies). This resonance occurrence also disappeared in the optimum motor as the natural frequency at the third elastic mode has been shifted to a higher frequency. The motor acceleration values at some other excitation forces' frequencies also have been shown and it can be seen that the motor vibration has decreased at these frequencies. The applied structural design caused the natural frequencies of the whole motor to increase (by increasing the stator's natural frequencies), so the optimum motor vibration levels, caused by the forces at different frequencies have been decreased (the motor stiffness is increased) as can be seen

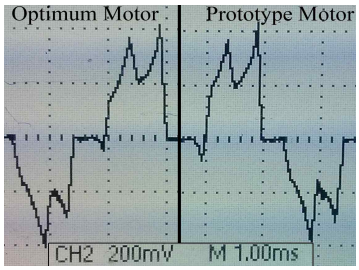

Fig. 13. The current waveforms of the two motor

in Fig. 11. The types of the excitation force components shown in Fig. 11 can be derived from Table 4.

Since the motor vibration characteristics are varied by some of the motor operational conditions like its speed and switching frequency, the vibration spectrum of the prototype and optimum motors have been measured and recorded at some other rotor speeds. The two motors vibration spectrums at the rotor speeds 1000, 2000 and 3000 rpm are presented in Fig. 12.

As can be seen in Fig. 12, the vibration spectrum amplitudes in the optimum motor have decreased at most of the frequency components for all of the rotor speeds. It shows that the proposed method can be effective at different rotor speeds besides the rated one. To give some examples showing the influences of applying the optimum holes on reducing or omitting the resonance effects, some points with their excitation force types, frequency and acceleration values are indicated in Fig. 12 (points 1 to 4).

Moreover, the experimental test results show that the two motors' performances (e.g. efficiency, output torque, speed, currents, etc.) are the same. For example, the current waveforms of the motors under a definite load are almost the same. The current waveforms are shown in Fig. 13.

5. Conclusion

An optimal structural design was introduced in this paper in order to increase the stator stiffness of a BLDC motor and to reduce its vibration by shifting the natural frequencies of the stator to higher values. Increasing the natural frequencies of the stator structure decreases the severe effects of the structural resonances, including high levels of noise and vibration, as the frequency components of the excitation forces in BLDC motors have lower magnitudes at higher frequencies. The proposed design method was based on placing a single hole on definite regions at the stator cross sectional area in such a way that no magnetic saturations and motor cogging torque enhancement occur. The optimum diameter and locations of the holes were extracted by RSM and the modal analyses in the iterative process were done by FEM. The optimum stator structure, with definite diameter and locations of the holes, was introduced. The natural frequencies of the optimum structure at different mode numbers increased about 190 to 250 Hz and its vibration displacements amplitude was 56% lower than the prototype stator structure. The performances of the prototype and the optimum motors were analyzed by FEM and the results showed that no magnetic saturation and cogging torque increment occur due to placing the optimum holes at the regions. The validity of the optimal design was tested and verified experimentally. The experimental results showed that the resonance occurrence in the prototype motor was disappeared in the optimum one by shifting the natural frequencies of the stator structure to higher values. Also, the motor vibration levels at different frequency components were decreased in the optimum motor. The FEM analysis and experimental test results also showed that placing the holes does not cause any negative effects on the motor performance.

References

[1] D. Y. Kim, J. K. Nam and G. H. Jang, "Reduction of Magnetically Induced Vibration of a Spoke-Type IPM Motor using Magnetomechanical Coupled Analysis and Optimization," *IEEE Trans. Magnetics*, vol. 49, no. 9, pp. 5097-5105, Sep. 2012.

[2] Hong-Seok Ko and Kwang-Joon Kim, "Characterization of Noise and Vibration Sources in Interior Permanent-Magnet Brushless DC Motors," *IEEE Trans. Magnetics*, vol. 40, no. 6, pp. 3482-3489, Nov. 2004.

[3] Sang-Ho Lee, Jung-Pyo Hong, Sang-Moon Hwang, Woo-Taik Lee, Ji-Young and Youbg-Kyoun Kim, "Optimal Design for Noise Reduction in Interior Permanent-Magnet Motor," *IEEE Trans. Industry Applications*, vol. 45, no. 6, pp. 1954-1960, Nov./Dec. 2009.

[4] D. Y. Kim, G. H. Jang and J. K. Nam, "Magnetically Induced Vibrations in an IPM Motor due to Distorted Magnetic Forces Arising from Flux Weakening Control," *IEEE Trans. Magnetics*, vol. 49, no. 7, pp. 3929-3932, Nov. 2013.

[5] Ji-Min Kim, Tao Sun, Sang-Ho Lee, Do-Jin Kim, Jung-Pyo Hong, "Evaluation and Improved Design about Acoustic Noise and Vibration in IPMSM," *in Proceeding of IEEE Electrical Machines and Systems Conference*, Incheon, South Korea, Oct. 2010.

[6] K. H. Yim, J. W. Jang, G. H. Jang, M. G. Kim, K. N. Kim, "Forced Vibration Analysis of an IPM Motor for Electrical Vehicles due to Magnetic Force," *IEEE Trans. Magnetics*, vol. 48, no. 11, pp. 2981-2984, Nov. 2012.

[7] P. Vijayraghavan and R. Krishnan, "Noise in Electric Machines: a Review," *IEEE Trans. Industry Applications*, vol. 35, no. 5, pp. 1007-1013, Apr. 1999.

[8] Jacek F. Gieras, Chong Wang and Joseph Cho Lai, Noise of Polyphase Electric Motors. Boca Raton, FL:

CRC Press, 2006.
[9] Jin Hur, Jin-Wook Reu, Byeong-Woo Kim and Gyu-Hong Kang, "Vibration Reduction of IPM-Type BLDC Motor Using Negative Third Harmonic Elimination Method of Air-Gap Flux Density," *IEEE Trans. Industry Applications*, vol. 47, no. 3, pp. 1300-1309, May/June 2011.
[10] Arthur W. Leissa, Vibration of Shells. New York, NY, USA: Acoustic Society of America, American Institute of Physics, 1993.
[11] Werner Soedel, Vibrations of Shells and Plates. NY: Marcel Dekker, 1993.
[12] S. J. Yang, Low-Noise Electrical Motors. Oxford, United Kingdom: Clarendon Press, 1981.
[13] Tao Sun, Ji-Min Kim, Geun-Ho Lee, Jung-Pyo Hong and Myung-Ryul Choi, "Effect of Pole and Slot Combination on Noise and Vibration in Permanent Magnet Synchronous Motor," IEEE Trans. Magnetics, vol. 47, no. 5, pp. 1038-1041, May 2011.

Mehrdad Jafaboland He received the B.S. and M.S. degrees in electrical engineering from Science and Industrial University in 1979 and Tarbiat Modares University in 1982, respectively. He received the PH.D. Degree in electrical engineering from Science and Research unit of Tehran University. After graduating, he became an associate professor in the electrical engineering Department of Malek-ashtar University of Technology.

Hossein Bagherian Farahabadi He received the B. Sc. and M. Sc. degrees in electrical engineering from Shahid Beheshti University, Tehran, Iran, in 2010 and 2012, respectively. He is currently working toward the Ph.D. degree in electrical engineering at Malek Ashtar University of Technology, Isfahan, Iran. His research interests include PM motors, power electronics and drives.